Numerical Computation of Unshielded Multiwires In-Cell Parameters for Coupling Between FDTD and MTL Methods Using Multipolar Expansions

Luis D. Angulo, Jesper Lansink Rotgerink, Harmen Schippers, *Member, IEEE*, Alberto Gascon Bravo, *Member, IEEE*, and Alejandro Muñoz Manterola

***Abstract*—This article presents a robust and efficient methodology to compute the per-unit-length in-cell inductance and capacitance matrices required to couple unshielded multiwire bundles to a 3-D finite-difference time-domain (FDTD) solver within a multiconductor transmission line framework. The proposed approach numerically solves the 2-D electrostatic and magnetostatic Laplace problems in an inner region and represents the field in the outer region by a multipolar (MP) expansion whose coefficients are computed from the full numerical solution. This hybrid finite element method (FEM)–MP formulation decouples the in-cell parameters from the specific FDTD cell position and size, avoids repeated numerical computations when bundles cross many cells, and naturally accommodates dielectric insulation. The method is validated on three cases of increasing complexity: 1) a single insulated wire; 2) two bare wires; and 3) a realistic 31-conductor bundle. Results are compared against a pure FEM reference, a boundary element method implementation and Bérenger's center-based approximation. The proposed FEM(inner)+MP(outer) scheme matches the FEM reference with very small discrepancies. The study also shows that conductor interactions shift the effective expansion centers away from geometric centers and that electrostatic and magnetostatic centers differ in the presence of dielectrics, which are effects not captured by simplified previous analytic models.**

***Index Terms*—Electrostatic solver, finite-difference time-domain (FDTD), numerical methods, transmission lines.**

I. Introduction

ELECTROMAGNETIC compatibility (EMC) analysis in aerospace and automotive platforms requires accurate models of transient electromagnetic fields that interact with complex wiring networks. These networks are typically composed of shielded or unshielded bundles (Fig. 1), each containing an arbitrary number of conducting wires, typically coated with a dielectric insulator. Solving submillimeter conductors and dense cable bundles together with a 3-D geometric model with full-wave solvers is computationally prohibitive, driving the development of a variety of hybrid strategies. One approach to this problem is based on field-to-transmission-line formulations to bridge theoretically any kind of 3-D field solver with multiconductor transmission line networks [1], [2].

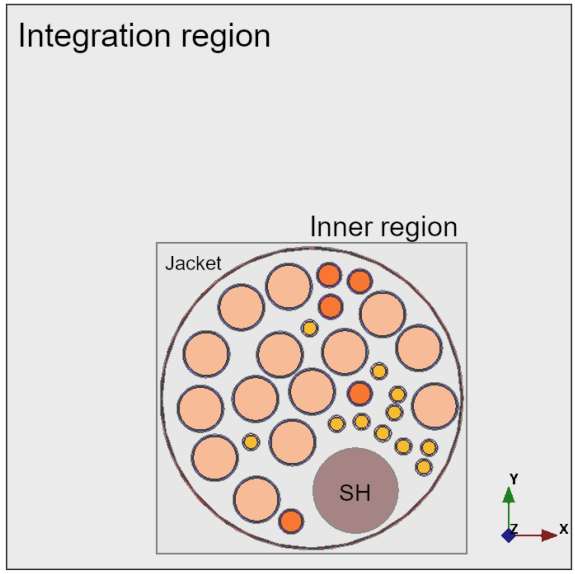


Fig. 1. Example of an unshielded multiwire bundle within an *integration region* required to compute its FDTD in-cell parameters. The bundle is composed of 31 round conductors, each surrounded by a dielectric except the one labeled with SH, which is an interior shielded bundle. The whole bundle is wrapped inside a jacket, which is modeled as a dielectric. The *inner region* inside the larger integration region will be used to compute the numerical in-cell capacitance and inductance values exactly, while in the remainder we evaluate the use of a MP expansion approach.

Specifically for the finite-difference time-domain (FDTD) method [3], contributions from several authors can be found. The coupling mechanism between a single wire and the 3D-FDTD discretized fields was introduced by Holland in [4] for wires aligned with the grid and by Guiffaut in [5] and [6] for oblique ones. For shielded multiwire bundles, Holland's method can be modified so the conductor now represents the shield of a multiwire bundle with its interior domain solved using an MTL

Received 8 February 2026; revised 10 April 2026 and 6 June 2026; accepted 10 July 2026. Date of publication 27 July 2026; date of current version 15 October 2026. This work was supported in part by the European Union under Grant 101101961-HECATE, in part by ESAMA under Grant PID2022-137495OB-C31 financed by MICIU/AEI/10.13039/501100011033, and in part by Open Access funding provided by Universidad de Granada / CBUA. *(Corresponding author: Luis D. Angulo.)*

Luis D. Angulo, Alberto Gascon Bravo, and Alejandro Muñoz Manterola are with the Department of Electromagnetism and State Matter Physics, University of Granada, 18071 Granada, Spain (e-mail: lmdiazangulo@ugr.es).

Jesper Lansink Rotgerink and Harmen Schippers are with Royal Netherlands Aerospace Centre, 1059 CM Amsterdam, Netherlands.

This article has supplementary material provided by the authors and color versions of one or more figures available at https://doi.org/10.1109/TEMC.2026.3713195.

Digital Object Identifier 10.1109/TEMC.2026.3713195

© 2026 The Authors. This work is licensed under a Creative Commons Attribution 4.0 License. For more information, see https://creativecommons.org/licenses/by/4.0/

formalism [7]. This formalism was demonstrated for a coaxial cable in [8] and for arbitrarily complex shielded bundles in [9]. The bundle's terminations can be modeled with lumped circuit solvers, such as `ngspice`, which are also coupled to the MTL problem, enabling the use of nonlinear [10] or dispersive [11] terminations; an example of the latter being common-mode chokes.

To solve unshielded multiwire bundles, Bérenger introduced in [12] a formalism in which the *in-cell parameters*, used to couple the MTL and FDTD equations, are computed for some simple arrangements of wires. The method is straightforward and only requires evaluating a single numerical integral. However, it needs to make several simplifying assumptions, such as assuming that a field distribution originates in the geometrical center of each wire, a hypothesis that does not generally hold due to the interactions between conductors. Bérenger's approach also does not provide a way to treat dielectrics, which makes it unapplicable to some of the complex bundles often encountered in industrial applications, such as the one represented in Fig. 1. To address this, Guiffaut [6] extended the method to include dielectric insulation, although only for a single wire. A more general approach was proposed by some of the authors of this work in [13], in which a finite element method (FEM) solver was used to calculate the required in-cell parameters. While this approach can handle the required complexity and produces results similar to Bérenger's for comparable cases, there are still some challenges when we aim to combine it with a general 3D-FDTD solver. First, FDTD meshes could contain many different cell sizes when rectilinear grids are used. Second, the method requires integrating over several different regions centered on the geometrical center of the wires. If not addressed, it would be required to numerically solve each possible combination of centers and cell sizes to compute all necessary in-cell parameters.

In this work, we will develop a methodology that allows overcoming these limitations by decomposing the computation of each in-cell parameter in three stages. In the first stage, we will use a numerical solver, in our case FEM, to handle the full complexity of the bundle. In the second stage, the numerical potential solution is used to determine coefficients of a multipolar (MP) expansion. Finally, the in-cell parameters for all FDTD cells can be computed by integrating the numerical solution over a common inner region and the MP expansion over various outer regions. This will limit the number of FEM solutions to be computed, as well as the required numerical integrations. In the numerical results section, a simple two-wire test case is compared in detail against Bérenger, FEM, and boundary integral equation (BIE) approaches, showcasing that the proposed approach preserves accuracy. A second test case shows that this remains true when dielectric insulation is included. Finally, a test case representing a real-world aircraft bundle, composed of 31 conductors, shows how well the proposed method performs on a complex, industrial-scale wire harness, both in terms of accuracy and computational efficiency. This case also highlights the need of a computational method for such dense bundles.

II. Per-Unit-Length Parameters for Multiwire Bundles

A. Unshielded Multiwires Within 3D-FDTD

Let us assume a multiwire bundle with N conductors contained in an unshielded region (Fig. 1) which is oriented along the $\hat{z}$-direction. To derive the in-cell parameters for this bundle, we assume that only a transverse electromagnetic mode propagates along its cross section [7]. This assumption is valid when the minimum wavelength of interest is much larger than the largest dimension of the bundle, allowing us to neglect the displacement current term in Maxwell's equations. In addition, due to its translational symmetry, we can neglect the spatial derivatives normal to the cross-section plane, i.e., the $\hat{z}$-direction. After removing these derivatives, Maxwell's equations decouple into two separate sets of equations: one relating the electric fields $\vec{E}$ and charge densities ρ, and another relating magnetic fields $\vec{H}$ and current densities $\vec{J}$. These define the electrostatic and magnetostatic 2-D problems, each governed by a 2-D Laplace equation. In the remainder of this work, we will primarily describe the electrostatic case, as the magnetostatic case is formally equivalent.

To obtain the in-cell parameters, let us follow an alternative derivation to [2], [4], [5], [6], [10], and [12] in which we will not require carrying an integral over an arbitrary radius. In the close neighborhood of the bundle, the electric field can be approximated by

$$\vec{E} = -\partial_x \phi \, \hat{x} - \partial_y \phi \, \hat{y} + E_z^i \, \hat{z} \tag{1}$$

where ϕ is the electric potential, and E_z^i represents a forcing field coming from external sources, i.e., not determined by the charges within the bundle. Introducing the magnetic potential $\vec{A} = (0, 0, A)$ and (1), we can write the x-component of the Faraday's law as

$$\partial_z \partial_y \phi - \partial_y E_z^i = \partial_t \partial_y A \tag{2}$$

which implies that the following differential equation must hold:

$$\partial_z \phi - E_z^i = \partial_t A. \tag{3}$$

The total electric and magnetic potentials in (3), at a given point, can be expressed as a superposition of potentials created by the sources on each of the N conductors. Therefore, it can be expressed in terms of these sources as

$$\phi(t, \vec{r}) = \sum_{n=1}^{N} Q_n(t, z) \, \tilde{\phi}_n(x, y) \tag{4a}$$

$$A(t, \vec{r}) = \sum_{n=1}^{N} I_n(t, z) \, \tilde{A}_n(x, y) \tag{4b}$$

with $\tilde{\phi}_n$ and $\tilde{A}_n$ being source-normalized bases of scalar fields, which can be obtained solving for the case in which the nth conductor is the only one with nonzero charge per-unit-length

Q_n or current I_n. Substituting (4) in (3) we obtain

$$\sum_{n=1}^{N} \tilde{\phi}_n \, \partial_z Q_n - \sum_{n=1}^{N} \tilde{A}_n \, \partial_t I_n = E_z^i \tag{5}$$

which, together with the charge continuity equation

$$\partial_t Q_n + \partial_z I_n = 0 \tag{6}$$

describes all charges per-unit-length and currents in all the wires in the bundle.

The coupling with the 3D-FDTD method is based on preserving (5) in a weak sense, doing several averages over the FDTD domain. We therefore define the *in-cell averaging operator* $\langle \cdot \rangle_m$ as an operator which can be applied on any scalar field $f(\vec{r})$, as

$$\langle f(\vec{r}) \rangle_m = \frac{\int_{S_m} f(\vec{r}) \, dS}{\int_{S_m} dS} \tag{7}$$

where

$$S_m = \left[x_m - \frac{\Delta x}{2}, x_m + \frac{\Delta x}{2} \right] \times \left[y_m - \frac{\Delta y}{2}, y_m + \frac{\Delta y}{2} \right] \tag{8}$$

is a rectangular domain centered at $\vec{r}_m = (x_m, y_m)$, with Δx and Δy representing the dimensions of the face at Yee's cell dual, which is crossed by the bundle.

Averaging (5) over N different domains S_m and rearranging terms, we obtain

$$\partial_t \mathbf{I} = -[\tilde{L}]^{-1} [\tilde{C}^{-1}] \, \partial_z \mathbf{Q} - [\tilde{L}]^{-1} \mathbf{E}^i_{z,\text{av}} \tag{9a}$$

$$\partial_t \mathbf{Q} = -\partial_z \mathbf{I} \tag{9b}$$

with $\mathbf{Q} = [Q_1, \ldots, Q_N]^T$, $\mathbf{I} = [I_1, \ldots, I_N]^T$, and where $\mathbf{E}^i_{z,\text{av}} = [\langle E_z^i \rangle_1, \ldots, \langle E_z^i \rangle_N]^T$ accounts for the contributions of the surrounding electric field. The terms $[\tilde{L}]$ and $[\tilde{C}^{-1}]$ are matrices containing the in-cell inductances per-unit-length and inverse in-cell capacitances per-unit-length, respectively, with each entry defined as

$$\left[\tilde{L}\right]_{mn} = \left\langle \tilde{A}_n(\vec{r}) \right\rangle_m \tag{10a}$$

$$\left[\tilde{C}^{-1}\right]_{mn} = \left\langle \tilde{\phi}_n(\vec{r}) \right\rangle_m \tag{10b}$$

and in which the origin of potential is set at conductor m.

Equations (9) provide the mechanism to couple field computations by the 3D-FDTD method, to currents on the cables. The computation of in-cell inductances and capacitances in (10) requires the use of (7) in which each integration domain S_m will be centered at a different point. To do this, Bérenger [12] used the geometrical center of each wire and analytical expressions to carry out the integration. While this approach is valid for an isolated wire, it is less accurate for multiwires as it neglects the influence of other conductors on the potential fields. Therefore, we will evaluate the use of alternative points that may be more suitable for bundle arrangements. Further discussion on this can be found in Section III-C.

As a final remark, it is worth noting that, in the absence of dielectrics, we can recover the well-known relationship

$$[\tilde{L}]_{mn} [\tilde{C}]_{mn} = \varepsilon_0 \mu_0. \tag{11}$$

B. Laplace Problem Definition

To compute (10a) and (10b) we start by defining the problem domain Ω as a union of a vacuum region Ω_0 with ε_0 and dielectric regions Ω_d with ε_d. The domain boundaries $\partial\Omega$ comprise the boundaries of the N conductors, $\partial\Omega_n$ with $n = 1, \ldots, N$. We aim to find a solution for the electrostatic potential at every point in Ω. For regions outside the conductors, assuming that the charge density ρ is zero, we can define a scalar electric potential ϕ

$$\vec{E} = -\nabla\phi \tag{12}$$

which is the solution of

$$\nabla \cdot \varepsilon \nabla \phi = 0. \tag{13}$$

On $\partial\Omega_n$, using the divergence theorem and Gauss law, the total charge for the nth conductor Q_n can be calculated as

$$Q_n = -\int_{\partial\Omega_n} \vec{D} \cdot d\vec{S} \tag{14}$$

with

$$\vec{D} = \varepsilon \vec{E}. \tag{15}$$

Alternatively, we can substitute (12) and (15) into (14) to obtain

$$Q_n = \varepsilon \int_{\partial\Omega_n} \nabla\phi \cdot d\vec{S} = \int_{\partial\Omega_n} \varepsilon \frac{\partial\phi}{\partial n} dS = \int_{\partial\Omega_n} \rho dS. \tag{16}$$

The integrand $\varepsilon \partial\phi/\partial n$ in (16) is the surface charge density, which will be denoted by ρ.

To finish the problem definition, we need to define appropriate boundary conditions on $\partial\Omega$. On all the conductor surfaces we will impose constant potentials, denoted with ϕ_n^b, using Dirichlet boundary conditions with

$$[\phi(\vec{r})]_{\partial\Omega_n} = \phi_n^b. \tag{17}$$

Furthermore, the charges on the nth conductor Q_n need to be prescribed. Take for example the case of two wires that was also analyzed in [12] and [13]. If one of these wires is charged and the other floating, the boundary conditions are

$$[\phi(\vec{r})]_{\partial\Omega_1} = \phi_1^b = 0, Q_1 = 1 \tag{18}$$

for the charged wire and

$$[\phi(\vec{r})]_{\partial\Omega_2} = \phi_2^b = \phi_2, Q_2 = 0 \tag{19}$$

for the floating wire, where ϕ_2 still needs to be determined.

In general, for a multiwire bundle with N conductors, the problem to be solved is to determine a potential ϕ such that one conductor contains a specified charge, while the other ones are floating (i.e., they contain no charge). Let the nth conductor be charged. Then, the boundary conditions are as follows:

$$\phi|_{\partial\Omega_n} = 0 \text{ and } Q_n = \int_{\partial\Omega_n} \varepsilon \frac{\partial\phi}{\partial n} dS = 1 \tag{20}$$

and

$$\phi|_{\partial\Omega_m} = \phi_m^b \text{ and } Q_m = \int_{\partial\Omega_m} \varepsilon \frac{\partial\phi}{\partial n} dS = 0, \; m \neq n \tag{21}$$

where the floating potentials ϕ_m^b still need to be determined. In this article, two approaches are considered to find the potential

to this problem. The first approach uses BIE, and the second one uses a finite element solver. Both approaches solve the potential in the domain Ω.

For the magnetostatic case, the fields $\vec{B}$ and $\vec{H}$ can be solved in a similar way by defining a magnetic vector potential $\vec{A} = (0, 0, A)$ which is generated by $\vec{J} = (0, 0, J)$ and in which the only nonzero components are in the $\hat{z}$-direction.

III. Numerical Solution Methods

This section introduces three different solution methods to determine the potentials in (10). First, a boundary element method (BEM) is introduced, which implements a representation in terms of BIE of the problem statement in Section II-B . The advantage of BIE is that boundary conditions (20) and (21) can be directly implemented. However, for the determination of the averaged potentials in (10), the potential has to be evaluated on a grid in the FDTD cell. This may become computationally expensive when using BEM, except if BEM is only used for the interior region. For this article, the BEM was only implemented for the two wire case also analyzed in [12] and [13], to be able to validate the implementations of the other two proposed solution methods in this section. Second, an FEM is proposed. It is shown how FEM with only Dirichlet conditions can still achieve the proper solutions satisfying (20) and (21). Finally, an MP expansion method is introduced. This method approximates the potential distribution inside the exterior region in Fig. 1, to prevent the requirement to rerun FEM and averaging computations for each different FDTD cell that a cable bundle crosses. For the solution in the interior region, and the computation of polar moments, the MP method still depends on an FEM or BEM solution. Section IV will compare results of these three methods.

A. Boundary Integral Equations

The solution of the 2-D Laplace problem with boundary conditions (20) and (21) can be represented by the single-layer potential

$$\phi(\vec{r}) = S_\Gamma \rho(\vec{r}) + \phi_\alpha \tag{22}$$

with Γ the union of all boundaries $\partial\Omega_n$, i.e., $\Gamma = \partial\Omega_1 \cup \ldots \cup \partial\Omega_N$. The boundary integral operator S_Γ is given by

$$(S_\Gamma \rho)(\vec{x}) := \frac{1}{2\pi} \int_\Gamma \rho(\vec{y}) \, \log \|\vec{x} - \vec{y}\| \, ds_{\vec{y}}, \quad \vec{x} \in \Omega \tag{23}$$

where $\|\cdot\|$ denotes the Euclidean norm. In (22), ϕ_α is a so called offset potential, and ρ is surface charge density on Γ.

The offset potential ϕ_α, the surface charge density ρ, and the potentials on the boundaries of the floating conductors can be solved by applying the Dirichlet boundary conditions (20) and (21) to the representation of (22), as shown in [14]. This is shown as follows for the case of two conductors, as was considered by [12]. The potential that satisfies conditions (20) and (21) is obtained by the following weak formulation: Find $\rho_1 \in H^{-1/2}(\partial\Omega_1)$, $\rho_2 \in H^{-1/2}(\partial\Omega_2)$, ϕ_α, and ϕ_β such that

$$(\psi_1, S_{\partial\Omega_1}\rho_1 + S_{\partial\Omega_2}\rho_2)_1 + \phi_\alpha \, (\psi_1, 1)_1 = 0 \tag{24a}$$

$$(\psi_2, S_{\partial\Omega_1}\rho_1 + S_{\partial\Omega_2}\rho_2)_2 + (\phi_\alpha - \phi_\beta) \, (\psi_2, 1)_2 = 0 \tag{24b}$$

$$(1, \rho_1)_1 = Q_1 \tag{24c}$$

$$(1, \rho_2)_2 = 0 \tag{24d}$$

for all $\psi_1 \in H^{1/2}(\partial\Omega_1)$ and $\psi_2 \in H^{1/2}(\partial\Omega_2)$ with

$$(\rho, \nu)_i = \int_{\partial\Omega_i} \rho(\vec{y}) \nu(\vec{y}) \, ds_{\vec{y}}. \tag{25}$$

The BIE in (24) can be solved by a BEM. The surface charge densities ρ_1 and ρ_2 are approximated by piecewise constant functions using boundary element meshes on the boundaries of the conductors. The coefficients of the boundary integral can be computed following the approach in [15], by which a solution of the surface charge densities is obtained.

The required potential $\tilde{\phi}_1(\vec{r})$ to compute the in-cell capacitance following (10) can now be computed by solving (24) for $Q_1 = 1$, and then evaluate (22) with the obtained surface charge densities. This allows us to compute $\tilde{C}_{1,1}$. For the computation $\tilde{C}_{1,2}$, a similar weak formulation, as in (24), is set up, with the difference that a charge Q_2 is prescribed to the second conductor, i.e., in (24d), and a floating potential ϕ_β is prescribed to the first conductor, e.g., the $-\phi_\beta$ shifts to (24a). Solving these formulations yields again surface charges on both conductors, from which the required $\tilde{\phi}_2(\vec{r})$ is again evaluated by (22).

B. Finite Element Method

Another approach to solving the problem described in Section II is to use FEM. With this approach, the computational domain Ω is tessellated into a mesh formed by a collection of curved triangles Ω_h. The outermost boundaries of this domain represent open boundaries $\partial\Omega_a$, on which we set first-order asymptotic boundary conditions (ABC), implemented as [16]

$$\left[\frac{\partial\phi(\vec{r})}{\partial n}\right]_{\partial\Omega_a} = -\left[\frac{\phi(\vec{r})}{r\log(r)}\right]_{\partial\Omega_a}. \tag{26}$$

On this mesh, we approximate the electric potential using functions from a Sobolev finite element space of weighted first-order differentiable scalar interpolatory polynomials $v_{h,i} \in H^1(\Omega_h)$

$$\phi(\vec{r}) \simeq \phi_h(\vec{r}) = \sum_i \phi_{h,i} \, v_{h,i}(\vec{r}) = \boldsymbol{\phi_h}^T \boldsymbol{v_h}(\vec{\boldsymbol{r}}). \tag{27}$$

Expansion (27) can be used within a Galerkin procedure to solve (13) to obtain the following linear system of equations:

$$[\mathcal{A}] \, \boldsymbol{\phi_h} = \boldsymbol{b} \tag{28}$$

where $[\mathcal{A}]$ is the finite element matrix and $\boldsymbol{b}$ is the right-hand-side vector derived from the Dirichlet conditions.

To obtain a solution which allows us compute (10a) and (10b) we will need to use values for the floating potentials $\phi^f_{m\neq n}$ to be used as Dirichlet conditions in $\boldsymbol{b}$. To do so, we first define the p.u.l *generalized capacitance matrix* $\mathcal{C}$, described in [7], as an $N \times N$ matrix with entries

$$\mathcal{C}_{mn} = \left.\frac{Q_n}{\phi^b_m}\right|_{\phi^b_{n\neq m}=0}. \tag{29}$$

With this definition, charges on conductors and corresponding boundary potentials are related following the matrix equation:

$$\mathbf{Q} = [\mathcal{C}]\,[\phi_1^b, \ldots, \phi_N^b]^T. \tag{30}$$

Assume we want to know the floating potentials in the rest of the conductors when ϕ_1^b is prescribed and Q_1 and the rest of the potentials are unknown. We can rearrange (30) to obtain the following:

$$-\phi_1^b \begin{bmatrix} \mathcal{C}_{1,1} \\ \mathcal{C}_{2,1} \\ \vdots \\ \mathcal{C}_{N,1} \end{bmatrix} = \begin{bmatrix} -1 & \mathcal{C}_{1,2} & \ldots & \mathcal{C}_{1,N} \\ 0 & \mathcal{C}_{2,2} & \ldots & \mathcal{C}_{2,N} \\ \vdots & \vdots & \ddots & \vdots \\ 0 & \mathcal{C}_{N,2} & \ldots & \mathcal{C}_{N,N} \end{bmatrix} \begin{bmatrix} Q_1 \\ \phi_{1,2}^f \\ \vdots \\ \phi_{1,N}^f \end{bmatrix}. \tag{31}$$

Therefore, we can obtain the source-normalized potential from a linear combination of the N earlier computed Laplace solutions

$$Q_1\tilde{\phi}_1 = \phi_1^b\hat{\phi}_1(x,y) + \sum_{m\neq 1} \hat{\phi}_{m,1}^f\,\hat{\phi}_m(x,y) \tag{32}$$

where

$$\hat{\phi}_1(x,y) = \left[\frac{\phi(x,y)}{\phi_1^b}\right]_{\phi_{m\neq 1}^b=0} \tag{33}$$

is the potential-normalized field for which the 1st conductor is the only one with a nonzero Dirichlet condition. Systems of equations similar to (31) can be solved to obtain source-normalized potentials for the remaining conductors.

C. Multipolar Expansion

To obtain in-cell inductances (10a) and in-cell capacitances (10b), we need to perform the averaging operation (7) over several different domains (8), which depend on the specific FDTD cell and conductors involved. If we assume that, for complex and realistic cases, a numerical approach is required to obtain the potentials, this can present several challenges as follows.

1) If we compute $\tilde{L}$ and $\tilde{C}$ in advance to use them as inputs for the FDTD solver, we must know the FDTD grid in which the bundle will be located beforehand. In addition, if the grid is graded or rectilinear, we would need to provide different $\tilde{L}$ and $\tilde{C}$ for each cell size, limiting the reusability of the solutions.
2) Alternatively, we could compute (10a) and (10b) within the FDTD solver during its initialization, starting from precomputed potential field solutions. However, passing all this information might involve a significant amount of data, requiring the solver to handle details, such as the basis used, the mesh, etc.
3) If the numerical solution is obtained using FEM, as in [13], the numerical integral is typically carried out on full elements that share a boundary with the FDTD cell. This again requires *a priori* knowledge of the grid to be used.

To address these challenges, we propose an approach based on an MP expansion of the field potentials [17]. In this method, domain (8) is decomposed into two regions (Fig. 1): 1) the *inner region* Ω_i; and 2) the *outer region* $\Omega_{o,n}$, such that $\Omega_n = \Omega_i \cup \Omega_{o,n}$. The inner region is rectangular and fixed for all the different in-cell averages (7), and it must be fully enclosed within $\Omega_{o,n}$. For the cases studied in this work, we found good results by centering the inner region on the geometrical center of the bundle, with a base and height 25% larger than the bundle's bounding box. This decomposition allows us to write (7) as

$$\langle f(\vec{r})\rangle_n = \left(\int_{\Omega_n} dS\right)^{-1} \left(\int_{\Omega_i} f(\vec{r})\,dS + \int_{\Omega_{o,n}} f(\vec{r})\,dS\right) \tag{34}$$

where $f(\vec{r}) \in \{\phi(\vec{r}), A(\vec{r})\}$. The inner region does not depend on the size or center of Ω_n and can therefore be directly computed using the numerical solution available in the FEM solver by the procedure explained before. To evaluate the outer region integral, we note that $f(\vec{r})$, being much smoother than in the inner region, can be described by a 2-D MP expansion around the *expansion center*, $\vec{r}_c$

$$f(\vec{r}) = \frac{1}{2\pi\varepsilon_0}\left(a_0 \log\frac{1}{R} + \sum_{p=1}^{\infty} \frac{a_p\cos(p\,\theta) + b_p\sin(p\,\theta)}{R^p}\right) \tag{35}$$

with $\vec{R} = \vec{r} - \vec{r}_c$ and a_p and b_p being the 2^p-polar moments

$$a_p = \frac{1}{p}\sum_{n=1}^{N}\int_{\partial\Omega_n} \rho R^p\cos(p\,\theta)\,d\Omega \tag{36a}$$

$$b_p = \frac{1}{p}\sum_{n=1}^{N}\int_{\partial\Omega_n} \rho R^p\sin(p\,\theta)\,d\Omega \tag{36b}$$

computed by accounting for the source density ρ, surface charge density for the electrostatic potential or current density for the magnetic potential, over the N conductors in the bundle, regardless of their location in the inner region. The expansion center is the point around which the nonzero order moments vanish; for nonneutral systems with a total charge or current of μ, it can be obtained as

$$\vec{r}_c = \frac{1}{\mu}\sum_{n=1}^{N}\int_{\partial\Omega_n} (x\hat{x} + y\hat{y})\rho\,d\Omega. \tag{37}$$

This approach allows us to compute the integral over the outer domain in (34) by truncating (35) up to a predetermined order P. This avoids the need of knowing in advance the FDTD grid in which the model will be used, allowing reusability in any type of cell that the grid may present. Moreover, this decouples the in-cell parameters computation stage from the FDTD solver which only requires to implement a numerical integral of (35).

As a final remark, we note that the contributions of the nonzero moments are relatively small for a sufficiently large in-cell domain. In fact, if the center of charge coincides with the center of the domain, their contribution to the integral is exactly zero. However, as we will see in the results presented in Section IV, this is not generally the case.

IV. Numerical Results

As a numerical test, we present results for computing the in-cell parameters (10a) and (10b), comparing them with a purely

FEM approach similar to [13], which is used as a reference. This numerical experiment is conducted for three cases of increasing complexity as follows.

1) *Two Bare Wires:* Conductor 1 with a radius a_1 of 1 mm, centered at the origin, and conductor 2 with a radius a_2 of 10 mm, located at (20 mm, 0). The integration domain is a square centered at the origin with $\Delta x = \Delta y = 200\,\text{mm}$.
2) A single insulated wire with a radius a of 1 mm, coated with a dielectric of $\varepsilon_r = 3.5$ and a thickness of 1 mm, following [13]. The integration domain (8) is a square centered at the origin with $\Delta x = \Delta y = 15\,\text{mm}$.
3) A *realistic* bundle composed of 31 conductors with positions and sizes provided as a supplementary material. All insulation in this bundle uses $\varepsilon_r = 2.0$. The results are for a cell centered on conductor 1, (x_1, y_1), with $\Delta x = \Delta y = 30\,\text{mm}$.

Apart from comparing to the FEM solution, the results are also compared to Bérenger's solutions and a BEM implementation.

In the following, if reference is made to the MP expansion method, this implies that the potential in the exterior domain is computed by the method in Section III-C. The potential in the interior domain is computed by FEM. For the FEM and MP methods, the three cases were modeled using Elemwave's workbench [18] for FreeCAD [19]. Their geometries were exported as NURBS in `.step` format and meshed into third-order curved elements using the script [20], based on the `gmsh` mesher [21]. The resulting mesh, along with a problem description file describing the electromagnetic characteristics of the materials, forms the input for the `opensemba/tulip` solver [22], which implements the method described in Section III-B. For the realistic bundle, the `gmsh` mesh used a maximum element size of 1.5 mm and curvature-based refinement with approximately 100 elements per full turn of boundary curvature. The implementation is based on the modular finite elements methods (MFEM) [23] library and uses third-order basis functions for H^1, matching the mesh elements, and thus defining an isoparametric scheme. For all cases, an ABC is set on a disk with a diameter four times the diagonal of the bundle's bounding box. For the MP expansion method, results were obtained using up to fifth-order (2^5)-polar moments; however, the values for a_p and b_p for $p \neq 0$ were typically below 10^{-6} and had little impact on the final result.

A. Two-Wire Problem

The two-wire problem, also covered in [12] and [13], will be used for a detailed three-way comparison between all numerical methods described in the previous section. First, let us assume that wire 1 is the charged wire and wire 2 is the floating wire, while wire 1 is in the center of the computational domain. These are the conditions to compute $\tilde{C}_{1,1}$. Once the solution of the Laplace problem statement has been found, the potential can be evaluated along the x-axis. The result is shown in Fig. 2(a), where the computed potential is compared with the analytical solution of a single charged wire at the origin, which is also used by Bérenger, and is given by

$$\phi(r) = \frac{1}{2\pi} \log(r/a_1) \tag{38}$$

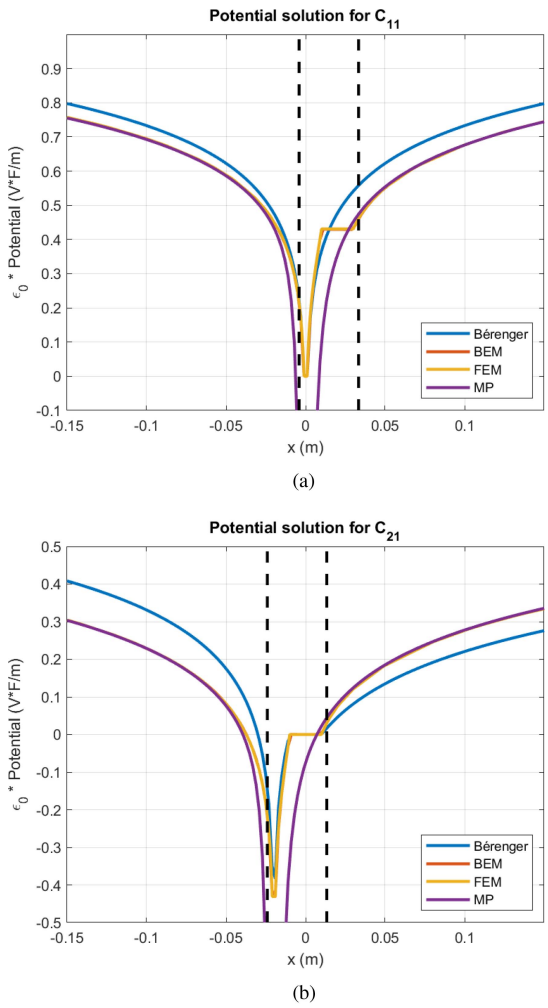


Fig. 2. Achieved potential solutions along the x-axis for conditions to compute (a) $\tilde{C}_{1,1}$ and (b) $\tilde{C}_{2,1}$. Dashed lines indicate the inner region.

with r being the distance to the origin. A similar result is shown in Fig. 2(b), for the conditions required for computation of $\tilde{C}_{2,1}$, e.g., a charged wire 1, and a floating conductor 2, where the latter is in the center of the domain.

This clearly shows that the BEM and FEM method yield similar solutions for the potential, and that also the MP expansion gives a valid approximation to the potential in the exterior region. Moreover, when compared to the analytical solution, the results confirm that the presence of the second wire has an effect on the potential distribution which is captured by the numerical methods, while this interaction is neglected by Bérenger's solution.

In the interior region, as expected, the MP solution deviates from the other solutions. The solved potentials are used to compute the resulting in-cell capacitance values, shown in Table I. Note that the table contains four numerically obtained results, for FEM and BEM, for the MP solution applied to the whole FDTD cell (Ω), and when FEM is applied to the interior region (Ω_1) and MP to the exterior region (Ω_2). The largest deviation is in the Bérenger result, compared to these numerical solutions, especially for $\tilde{C}_{11}$. This is again caused by the fact

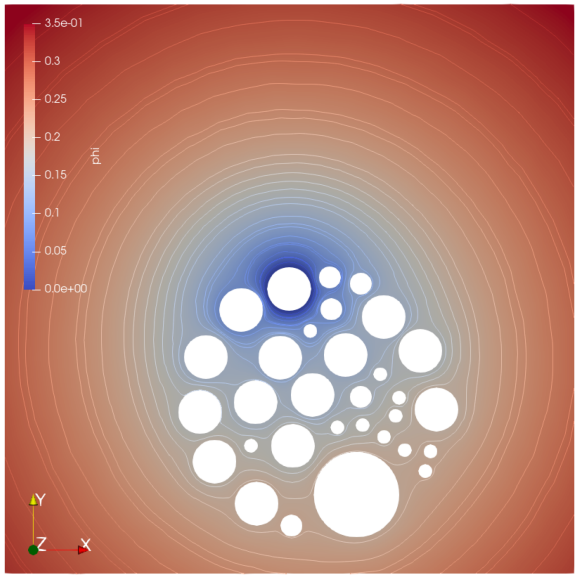


Fig. 3. Numerical solution of the potential-normalized field (33) used to compute $[\tilde{C}^{-1}]_{1,1}$ in (10b). The white circles represent the conductor interiors, where the potential is the same as at their boundaries. While the equipotential lines are complex in the immediate surroundings of the bundle (inner region), they approximate circumferences farther away, justifying the use of the MP expansion.

TABLE I
COMPARISON OF NUMERICAL SOLUTIONS FOR CAPACITANCES COMPUTED FOR THE TWO WIRE CASE

Parameter	Bérenger	FEM	BEM	MP(Ω)	FEM(Ω_1) + MP(Ω_2)
$\tilde{C}_{1,1}$(pF)	13.1306	14.0418	14.0880	14.1133	14.0448
$\tilde{C}_{2,1}$(pF)	44.3179	44.2014	44.2159	44.4809	44.1525

that Bérenger neglects the interaction between wires. The results computed by FEM, BEM, and the combination of FEM + MP are actually very close to each other. This shows that the methodology suggested in this article provides accurate results. The differences in the interior region for MP observed in Fig. 2, give rise to slight differences when using MP in the whole region Ω to compute the in-cell parameters. Still, this difference is smaller than 0.5%, implying that the averaging can be quite forgiving for small errors in the potential. In practice, this explains why the method remains accurate even when pointwise potential curves are not identical in the far field. When stricter agreement is required, the mismatch can be reduced by increasing the MP order or enlarging the inner region used for FEM. This yields the conclusion that the proposed method with MP solution in the exterior domain and FEM solution in the interior domain is a very good approach.

B. Single Insulated Wire and Realistic Bundle

In Table II, results for the single insulated wire and realistic bundle cases are compared for FEM, FEM+MP, Bérenger, and BEM. For the latter, two only inductance values are given, as both Bérenger and the used Matlab implementation of BEM are unable to handle effects of dielectrics to capacitance values

TABLE II
COMPARISON OF CAPACITANCE (pF) AND INDUCTANCE (nH) CALCULATIONS FOR INSULATED WIRE AND REALISTIC BUNDLE

Case	Parameter	FEM	FEM(Ω_1) + MP(Ω_2)	BEM	Bér.	RE
Insulated wire	$\tilde{C}_{1,1}$	47.40	47.32	-	46.92	0.16
	$\tilde{L}_{1,1}$	330.84	331.17	330.72	330.77	-0.10
Realistic Bundle	$\tilde{C}_{1,1}$	40.92	40.66	-	-	0.63
	$\tilde{C}_{1,17}$	125.48	126.53	-	-	-0.84
	$\tilde{C}_{1,26}$	59.06	58.87	-	-	0.33
	$\tilde{C}_{1,31}$	177.97	180.52	-	-	-1.43
	$\tilde{L}_{1,1}$	299.90	300.01	299.80	440.51	-0.04
	$\tilde{L}_{1,17}$	87.46	86.55	87.62	80.05	1.04
	$\tilde{L}_{1,26}$	202.34	202.51	202.58	309.65	-0.08
	$\tilde{L}_{1,31}$	59.65	58.36	59.70	27.08	2.15
	$\tilde{L}_{17,17}$	426.83	426.25	426.38	672.38	0.14
	$\tilde{L}_{17,31}$	137.28	137.03	137.60	212.11	0.19

TABLE III
INDICATIVE RUNTIMES FOR FEM SOLVER STAGE, COMBINED FEM + MP, AND A FULL FEM SOLUTION

Case	FEM solve	FEM+MP	FEM-only equiv.
Single insulated wire	0.81 s	1.04 s	0.81 s
Two wires	18.3 s	25.2 s	36.6 s
31-conductor bundle	1.4 min	4.9 min	42 min

(with the exception of an available analytical expression for the single wire case). In line with the comparisons made in the previous section, all numerical approaches are very similar. The table gives relative errors (RE) in % relating FEM to FEM+MP, which are typically below 0.2 % for the single wire and 0.85 % for the realistic bundle case. For the realistic bundle, only the values of $\tilde{C}_{1,31}$ and $\tilde{L}_{1,31}$ are higher because they correspond to the large conductor representing the shield of an inner bundle, which is also relatively close to the inner region boundary. When wire 17 is placed in the middle, for $\tilde{C}_{17,17}$ and $\tilde{C}_{17,31}$ the values of the numerical codes match very well, but are very different from Bérenger's solutions. This illustrates that for such densely packed bundles with varying wire sizes, Bérenger's results cannot be trusted.

This industrial-scale test case also highlights the added benefit of the presented FEM+MP methodology in terms of computational complexity, as shown by Table III. Measured on one core of an AMD Ryzen Threadripper 7960X, it reports the FEM solve time, the FEM+MP calculation cost of one full run, and the FEM-only equivalent. For the pure-FEM strategy applied to the 31-conductor bundle, the solver would have to be re-run for each distinct cell configuration, whereas with the proposed approach the FEM solve and MP coefficient extraction are performed once per conductor and reused across all FDTD cells. Once the MP coefficients are available, only a cheap line integral over the MP expansion is needed per FDTD cell. The per-run cost is dominated by the cost of solving (24) and (28) for BEM and FEM methods, respectively. For a bundle with N_W wires the system must be solved N_W^2 times, once for each wire and once with a cell centered on each wire. In the hybrid FEM+MP approach, the FEM solve and MP coefficient extraction are each

required N_W times during setup; per FDTD cell, the outer region contribution reduces to a much cheaper numerical integration using the precomputed MP terms. Moreover, the same FEM solution is reused for all FDTD cells crossed by the meters-long bundle, while for the pure-FEM strategy on each FDTD cell N_W^2, new FEM solutions will have to be computed.

As a final remark, we note that the expansion centers do not generally coincide with the geometric centers of the wires in cases with more than one wire. For the two-wire case, the geometric center of conductor 1 is (0, 0), while the expansion centers for the electrostatic and magnetostatic cases are $(5\,\mathrm{mm}, 0)$. In the realistic case, the geometric center of conductor 1 is $(-1.209\,\mathrm{mm}, 5.934\,\mathrm{mm})$, while the expansion centers are $(-0.638\,\mathrm{mm}, 2.890\,\mathrm{mm})$ and $(-0.686\,\mathrm{mm}, 3.031\,\mathrm{mm})$ for the electrostatic and magnetostatic expansions, respectively. This result indicates that the interaction between the conductors is nonnegligible, contrary to the simplifying hypothesis in [12].

V. Conclusion

In this article, we present a hybrid methodology that computes in-cell inductance and capacitance matrices for unshielded multiwire bundles by solving the Laplace problems with FEM in an inner region and applying an MP expansion in the outer region. This strategy decouples the parameters from specific FDTD cell positions and sizes, avoids repeated computations when bundles traverse many cells, and naturally incorporates dielectric insulation. Once an FEM solution is computed and its MP coefficients are obtained, the result is reused for many outer-cell integrations without repeating full FEM solves. Validation on a single insulated wire, two bare wires, and a realistic 31-conductor bundle showed excellent agreement with a pure FEM reference and, for the two-wire case, with BEM, while improving on center-based analytical approximations. Quantitatively, the hybrid FEM(inner)+MP(outer) scheme achieves small discrepancies (e.g., RE of 0.16% for capacitance and 0.10% for inductance on the single wire, and typically below 0.85% with a maximum of 2.15% for the realistic bundle). The analysis highlights that conductor interactions shift effective expansion centers away from geometric centers and that electrostatic and magnetostatic centers differ in the presence of dielectrics. Overall, the approach preserves FEM accuracy while delivering reusable, cell-agnostic in-cell parameters suitable for industrial-scale FDTD–MTL co-simulation in EMC applications. The method is most reliable when the inner boundary is sufficiently separated from conductors and when enough MP terms are retained for the desired tolerance. Experimental and simulation cross-comparison of the FDTD–MTL framework employing these in-cell parameters was demonstrated in [24], which uses the present method to extract per-unit-length inductances and capacitances and reports good agreement with time-domain measurements on a cable–panel test fixture under lightning-like excitation, confirming the practical reliability of the proposed approach.

References

[1] A. K. Agrawal, H. J. Price, and S. H. Gurbaxani, "Transient response of multiconductor transmission lines excited by a nonuniform electromagnetic field," *IEEE Trans. Electromagn. Compat.*, vol. EMC-22, no. 2, pp. 119–129, May 1980.

[2] J.-P. Parmantier et al., "Modelling EM-coupling on electrical cable-bundles with a frequency-domain field-to-transmission line model based on total electric fields," *Adv. Electromagnetics*, vol. 9, no. 3, pp. 15–31, Dec. 2020. [Online]. Available: https://aemjournal.org/index.php/AEM/article/view/1531

[3] A. Taflove, A. Oskooi, and S. G. Johnson, *Advances in FDTD Computational Electrodynamics: Photonics and Nanotechnology*. Norwood, MA, USA: Artech House, 2013.

[4] R. Holland and L. Simpson, "Finite-difference analysis of EMP coupling to thin struts and wires," *IEEE Trans. Electromagn. Compat.*, vol. EMC-23, no. 2, pp. 88–97, May 1981.

[5] C. Guiffaut, A. Reineix, and B. Pecqueux, "New oblique thin wire formalism in the FDTD method with multiwire junctions," *IEEE Trans. Antennas Propag.*, vol. 60, no. 3, pp. 1458–1466, Mar. 2012.

[6] C. Guiffaut, N. Rouvrais, A. Reineix, and B. Pecqueux, "Insulated oblique thin wire formalism in the FDTD method," *IEEE Trans. Electromagn. Compat.*, vol. 59, no. 5, pp. 1532–1540, Oct. 2017.

[7] C. R. Paul, *Analysis of Multiconductor Transmission Lines*. Hoboken, NJ, USA: John Wiley & Sons, Inc., 2007.

[8] M. Feliziani and F. Maradei, "Full-wave analysis of shielded cable configurations by the FDTD method," *IEEE Trans. Magn.*, vol. 38, no. 2, pp. 761–764, Mar. 2002.

[9] A. G. Bravo et al., "Hybridization of full-wave FDTD solver with a multilevel multiconductor transmission line solver with ngspice interconnections," in *Proc. Int. Symp. Electromagn. Compat.*, 2025, pp. 440–445.

[10] A. Ga. Bravo, L. M. D. Angulo, F. Silva, M. Quílez, K. Tekbaş, and S. G. Garcıá, "Hybridization of multiconductor transmission line solver with circuit solver ngspice to treat line interconnections and terminations," *IEEE Trans. Electromagn. Compat.*, vol. 67, no. 3, pp. 931–939, Jun. 2025.

[11] A. G. Bravo et al., "Time domain simulation of common mode ferrite chokes at system level," *IEEE Trans. Electromagn. Compat.*, vol. 65, no. 6, pp. 1900–1908, Dec. 2023.

[12] J.-P. Berenger, "A multiwire formalism for the FDTD method," *IEEE Trans. Electromagn. Compat.*, vol. 42, no. 3, pp. 257–264, Aug. 2000.

[13] J. L. Rotgerink, H. Schippers, A. G. Bravosup, L. D. Angulo, and S. G. García, "Numerical computation of in-cell parameters for multiwire formalism in FDTD," in *Proc. Int. Symp. Electromagn. Compat.*, 2024, pp. 334–339.

[14] D. Amann, A. Blaszczyk, G. Of, and O. Steinbach, "Simulation of floating potentials in industrial applications by boundary element methods," *J. Math. Ind.*, vol. 4, 2014, Art. no. 13, doi: 10.1186/2190-5983-4-13.

[15] G. Hsiao, P. Kopp, and W. Wendland, "A Galerkin collocation method for some integral equations of the first kind," *Computing*, vol. 25, pp. 89–130, 1980, doi: 10.1007/BF02259638.

[16] J. Jin, *The Finite Element Method in Electromagnetics*. Hoboken, NJ, USA: Wiley-Interscience, 1993.

[17] T. Gantumur, "Multipole expansions in the plane," 2016. [Online]. Available: https://www.math.mcgill.ca/gantumur/math319w16/multipole2d.pdf

[18] "Elemwave's workbench," Elemwave, Granada, Spain, 2025. [Online]. Available: https://www.elemwave.com

[19] FreeCAD Team, "FreeCAD," 2024, open source parametric 3D modeler. [Online]. Available: https://www.freecad.org/

[20] L. D. Angulo, A. M. Manterola, and A. Gascon Bravo, "opensemba/step2gmsh: MFEM compatible meshes from step files," Jun. 2023. [Online]. Available: https://github.com/opensemba/step2gmsh

[21] C. Geuzaine and J.-F. Remacle, "Gmsh: A 3-D finite element mesh generator with built-in pre-and post-processing facilities," *Int. J. Numer. Methods Eng.*, vol. 79, no. 11, pp. 1309–1331, 2009.

[22] L. D. Angulo, A. M. Manterola, and A. Gascon Bravo, "opensemba/tulip: Opensource per unit length multiconductor transmission line and in-cell parameters solver," Jun. 2023. [Online]. Available: https://github.com/opensemba/tulip

[23] "MFEM: Modular finite element methods [Software]," [Online]. Available: mfem.org

[24] A. Gascon Bravo et al., "A study of nonlinear effects on an aircraft electrical-structure network mockup," in *Proc. Int. Symp. Electromagn. Compat.*, Oct. 2026.